

element 108. Report P7-86-322, page 26 (Joint Institute for Nuclear Research, JINR, Dubna, 1986) (in Russian).

18. Dougan, R. J., Moody, K. J., Hulet, E. K. & Bethune, G. R. OSCAR: An apparatus for on-line gas-phase separations. FY87 Annual Report UCAR 10062/87, 4–17 (Lawrence Livermore National Laboratory, LLNL, Nuclear Chemistry Division, Livermore, 1987).
19. Pershina, V., Bastug, T., Fricke, B. & Varga, S. The electronic structure and properties of group 8 oxides MO<sub>3</sub>, where M = Ru, Os, and element 108, Hs. *J. Chem. Phys.* **115**, 792–799 (2001).
20. Düllmann, Ch. E., Eichler, B., Eichler, R., Gäggeler, H. W. & Türler, A. On the stability and volatility of group 8 tetroxides MO<sub>4</sub> (M = ruthenium, osmium, and hassium (Z = 108)). *J. Phys. Chem. B* **106**, 6679–6684 (2002).
21. Düllmann, Ch. E. *et al.* IVO, a device for in situ volatilization and on-line detection of products from heavy ion reactions. *Nucl. Instrum. Meth. A* **479**, 631–639 (2002).
22. Kirbach, U. W. *et al.* The cryo-thermochromatographic separator (CTS): A new rapid separation and  $\alpha$ -detection system for on-line chemical studies of highly volatile osmium and hassium (Z = 108) tetroxides. *Nucl. Instrum. Meth. A* **484**, 587–594 (2002).
23. Malmbeck, R. *et al.* Separation of <sup>248</sup>Cm from a <sup>252</sup>Cf neutron source for production of Cm targets. *Radiochim. Acta* **89**, 543–549 (2001).
24. Zvara, I. Thermochromatographic method of separation of chemical elements in nuclear and radiochemistry. *Isotopenpraxis* **26**, 251–258 (1990).
25. Zvara, I. Simulation of thermochromatographic processes by the Monte Carlo method. *Radiochim. Acta* **38**, 95–101 (1985).

**Acknowledgements**

We thank the staff of the Laboratory for Micro- and Nanotechnology at PSI for manufacturing the PIN-diode sandwiches for the COLD array and the staff of the GSI UNILAC for providing stable, highly intense beams of <sup>26</sup>Mg as well as the target laboratory for Be foils for the vacuum windows. Support from the European Commission Institute for Transuranium Elements, Karlsruhe, for long-term storage of <sup>252</sup>Cf and the chemical separation of <sup>248</sup>Cm is appreciated. These studies were supported in part by the Swiss National Science Foundation and the Chemical Sciences Division of the Office of Basic Energy Sciences, US Department of Energy.

**Competing interests statement**

The authors declare that they have no competing financial interests.

Correspondence and requests for materials should be addressed to H.W.G. (e-mail: gaeggeler@iac.unibe.ch).

**Mantle compensation of active metamorphic core complexes at Woodlark rift in Papua New Guinea**

**Geoffrey A. Abers\***, **Aaron Ferris\***, **Mitchell Craig†‡**, **Hugh Davies†**, **Arthur L. Lerner-Lam§**, **John C. Mutter§** & **Brian Taylor||**

\* Department of Earth Sciences, Boston University, Boston, Massachusetts 02215, USA  
 † Department of Geology, University of Papua New Guinea, Port Moresby, Papua New Guinea  
 § Lamont-Doherty Earth Observatory of Columbia University, Palisades, New York 10964, USA  
 || University of Hawaii, Manoa, Hawaii 96822, USA

In many highly extended rifts on the Earth, tectonic removal of the upper crust exhumes mid-crustal rocks, producing metamorphic core complexes. These structures allow the upper continental crust to accommodate tens of kilometres of extension<sup>1</sup>, but it is not clear how the lower crust and underlying mantle respond. Also, despite removal of the upper crust, such core complexes remain both topographically high and in isostatic equilibrium. Because many core complexes in the western United States are underlain by a flat Moho discontinuity<sup>2,3</sup>, it has been widely assumed that their elevation is supported by flow in the lower crust<sup>4–6</sup> or by magmatic underplating<sup>7</sup>. These processes should decouple upper-crust extension from that in the mantle.

‡ Present address: Department of Geological Sciences, California State University, Hayward, California 94542, USA.

In contrast, here we present seismic observations of metamorphic core complexes of the western Woodlark rift that show that the overall crust is thinned beneath regions of greatest surface extension. These core complexes are actively being exhumed<sup>8</sup> at a rate of 5–10 km Myr<sup>-1</sup>, and the thinning of the underlying crust appears to be compensated by mantle rocks of anomalously low density, as indicated by low seismic velocities. We conclude that, at least in this case, the development of metamorphic core complexes and the accommodation of high extension is not purely a crustal phenomenon, but must involve mantle extension.

The Woodlark rift of Papua New Guinea (Fig. 1) is the site of some of the youngest, most recently uplifted metamorphic core complexes (MCCs) on the planet<sup>8</sup>, and the most rapidly extending continental crust<sup>9</sup>. Extension began producing new sea floor along strike by 5–6 Myr ago<sup>10</sup>, leading to MCC exhumation on Ferguson and Goodenough islands in the Pliocene epoch, as indicated by sediment composition in adjacent basins<sup>8</sup>. Most workers infer that extension is driven by plate forces such as slab pull at other margins of the Solomon Sea<sup>11</sup> or by gravitational collapse<sup>10</sup>, similar to some large-extension rifts elsewhere but contrasting with active rifts such as the east Africa rift<sup>12,13</sup>. Magnetic lineations require 100–200 km extension across the D’Entrecasteaux MCCs<sup>10</sup>, at 20–35 mm yr<sup>-1</sup>, much of which must be accommodated on the north-dipping detachment shear zones bounding them. The MCCs show rapid uplift, with footwall rocks having experienced conditions of 700–900 °C and 5–6 kbar as recently as 3–4 Myr ago, and 4–5 kbar at similar temperatures at 1.5–2 Myr ago<sup>14,15</sup>. The MCCs seem to be at present exhuming, as indicated by geomorphic<sup>16</sup> and low-temperature geochronological indicators<sup>14</sup>.

In 1999 and 2000, we placed 19 broadband seismographs at 11 sites across the western Woodlark rift (Fig. 1), from the relatively unextended Papuan peninsula in the south, across the D’Entrecasteaux MCCs, to the northern edge of the Trobriand platform. Data recorded by these stations provide, to our knowledge, the first available constraints on the deep structure of this rift.

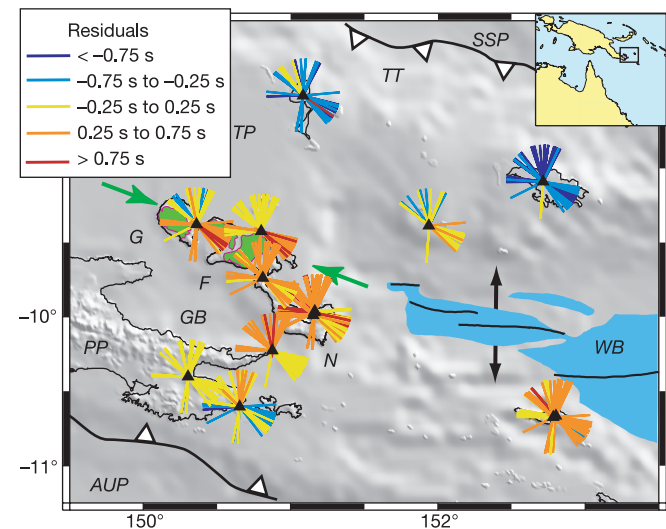


**Figure 1** Tectonic features of the western Woodlark rift, showing seismic stations (small black triangles) and azimuths of incident teleseismic rays. Blue shaded region, new sea floor (<2 Myr old); black arrows, direction of modern extension; green arrows, chain of MCCs. Letters denote the D’Entrecasteaux islands: Goodenough (G), Ferguson (F) and Normanby (N); the Papuan peninsula (PP), Goodenough basin (GB), Trobriand platform (TP), Trobriand trough (TT), Woodlark basin (WB), Australian plate (AUP), and Solomon Sea plate (SSP). Lines radiating from stations point at back-azimuth of incident teleseismic P waves, and indicate travel time residuals by colour. Blue lines, indicating negative residuals, show seismically fast regions while red regions indicate slow regions.

Teleseismic P coda constrains crustal thickness via receiver function techniques<sup>17</sup>. We generate receiver functions from the Woodlark broadband signals and invert for crustal structure (Figs 2 and 3; see Methods for details). The results document large variation in crustal thickness: beneath the relatively unextended Papuan peninsula, crustal thickness is 10–15 km greater than beneath the D’Entrecasteaux islands, 50–100 km to the north. The thinnest crust, 20 km thick, lies beneath Normanby island close to the oceanic rift tip, and crust remains thin beneath all D’Entrecasteaux stations. Crust thickens to the north, although a large gap in coverage obscures details of this transition, and the >40 km thickness at the northernmost station may include 6–8 km of oceanic crust underthrust southward from the Trobriand trough. Beneath some stations Moho depths show azimuthal variations in excess of 5 km, perhaps due to dipping Moho structure or unmodelled anisotropy; these complexities do not affect the overall Moho geometry, and so are not considered further. The regional pattern suggests that extension occurs where crust thins. This contrasts with the flat Moho beneath the transition between the Basin and Range and the Colorado Plateau<sup>3</sup>. Beneath the D’Entrecasteaux islands, the average Moho upwarp is 10–15 km, close to the amount of upper crust tectonically removed over the MCCs in the past 2 Myr, a correlation that suggests a causal link. Mid-crustal discontinuities could not be identified beneath most stations, so variations in lower-crustal thickness could not be directly measured.

The observed crustal thinning of 10–15 km should produce 1.5–3 km of subsidence, if isostatically balanced, depending upon whether or not the mantle lithosphere thins in concert with the crust (Fig. 4b). However, average elevations throughout the D’Entrecasteaux islands lie close to sea level, as do elevations at the end of the Papuan peninsula. Also, Bouguer gravity anomalies (Fig. 4c) indicate isostatic compensation. Hence, some other source of buoyancy must exist to support topography. To test the possibility that isostatic support comes from the mantle, we measure travel-time residuals in teleseismic P waves (Fig. 1). Residuals at stations on the north flanks of the MCCs show up to 1 s variation with azimuth, which requires a substantial velocity variation across this tectonic boundary (>5% if distributed uniformly over the upper 150 km); other stations on the MCCs are consistently slow,

requiring lower wave speeds in the mantle beneath the D’Entrecasteaux Islands than elsewhere. To illuminate the source of these residuals, we formally invert them for P velocities.

Inversion delineates slow velocities in the uppermost mantle associated with the D’Entrecasteaux islands and the oceanic rift, and faster velocities elsewhere (Figs 3 and 4a). These anomalies are strongest within the upper 100 km, with the uppermost mantle beneath the D’Entrecasteaux islands ~5% slower than surrounding material. Such variations are apparent in the pattern of residuals (Fig. 1), and show that at mantle depths the low-velocity region at the oceanic rift tip is contiguous with low velocities beneath these islands. The anomalies, if interpreted in terms of temperature alone, require 300–700 °C higher temperatures depending upon the effects of attenuation; the 700 °C value ignores possible physical dispersion effects<sup>18</sup>, and so provides an upper bound. Such high temperatures probably require melting. This is indeed likely, given the geologic evidence of Plio-Quaternary volcanism and granodiorite intrusion in the area<sup>19</sup>.

To describe the isostatic consequence of these anomalies, we compare the predicted gravity anomalies from both the crustal root and the mantle velocity structure to observed gravity (Fig. 4c). The only parameters adjusted to fit observed gravity are a constant term to account for long-wavelength effects, and two parameters describing plate flexure between the northernmost constraint and the Trobriand trough ( $X = 170$ – $250$  km, where  $X$  is horizontal distance on Fig. 4). The predicted positive anomaly from the elevated Moho (replacing crust with mantle) shows the same amplitude and shape, but opposite sign, as that predicted from the mantle velocity structure. Hence, by Gauss’s theorem, the excess mass associated with thinned crust across the D’Entrecasteaux islands equals the mass deficit of the upper mantle. No additional lateral density anomalies need be present to compensate topography. The observed gravity deviates by ~40 mGal from the predicted combination of both effects at wavelengths of ~250 km, perhaps reflecting dynamic effects, long-wavelength density variations, or errors in assumed velocity–density relationships (see Methods).

These observations show rifting at the onset of continental

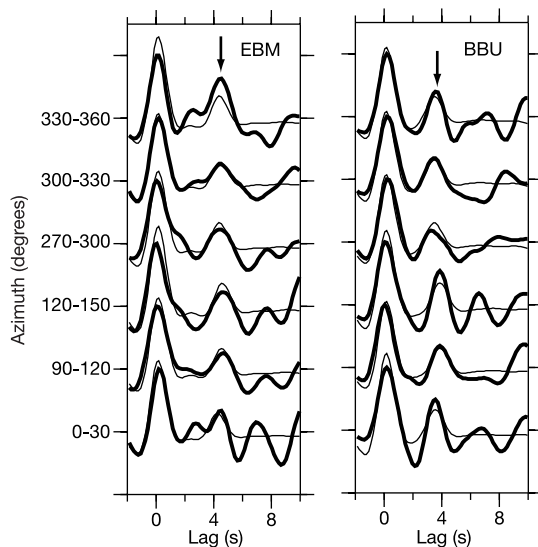


**Figure 2** Receiver functions from two stations (EBM and BBU; see Fig. 3), stacked over 30° azimuthal bins. Thick lines, observed receiver functions; thin lines, best fit from inversion. The strong positive peak at 0 s corresponds to the direct P arrival, while the arrival at 3–5 s is the P-to-S conversion (Ps) off the Moho (arrow). Variations in Ps arrival time between stations reflect variation in crustal thickness.

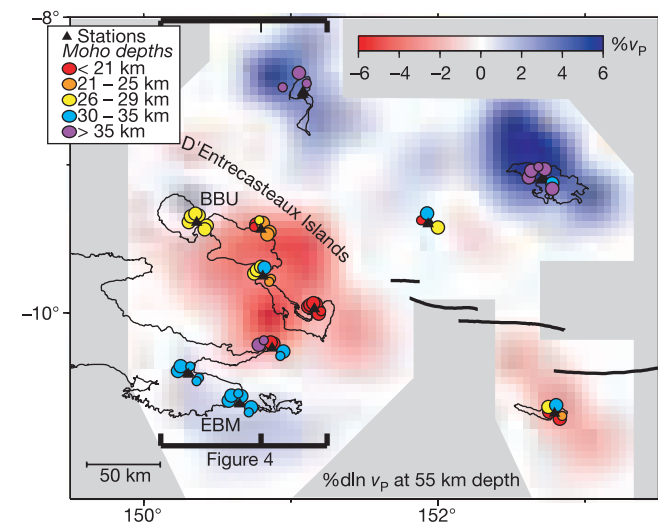


**Figure 3** Imaging results beneath the western Woodlark rift. Colours show the percentage change to  $v_p$  from inversion of teleseismic P waves, at a depth of 55 km (uppermost mantle). Grey area, region of negligible resolution (resolution matrix diagonals  $< 0.1$ ). Coloured circles, depths to Moho estimated from receiver function inversions, plotted for each stack at average location of Ps conversion off Moho; smaller size indicates 95% confidence limits  $> 10$  km. Brackets, location of profile on Fig. 4. Triangles, seismic stations; thick line, location of active spreading segment. Note good correlation between slow regions (red) and thin crust, in particular the low-velocity region beneath the D’Entrecasteaux islands.

breakup in which MCCs form above the area of crustal thinning. In this region, mantle buoyancy and not crustal thickening isostatically supports regionally positive elevations for the D'Entrecasteaux islands region. Some second-order variations in lower-crustal thickness must explain along-strike variations in Moho depth beneath the MCCs, either through lower-crustal flow, magmatic addition, or variations in pre-extensional crustal thickness. Also, some flow of lower crust may be needed to explain subsidence and heat flow of basins adjacent to the D'Entrecasteaux islands<sup>20</sup>. These along-strike changes in crustal thickness appear to be compensated through mantle heating, like the across-strike variations, as crustal thickness correlates with mantle velocities (Figs 1 and 3). Overall, the wholesale transfer of lower crust from unextended to highly

extended regions, inferred as the primary response to extension in the western US<sup>5,6</sup>, need not be invoked here.

Several differences exist between the Woodlark rift and other rifts that may explain the juxtaposed thinning of crust and mantle lithosphere. Active continental rifts, such as the east Africa rift, similarly show large mantle heating<sup>13,21</sup> but less than 20 km total surface extension, so provide little information on how the lithosphere responds to large extension. Only the western US and the Aegean region show comparable modern extension rates<sup>9</sup>, but both have relatively flat Mohos. One possibility is that pre-existing structure favours localization of crustal thinning at Woodlark, such as crust and mantle weakening from the Trobriand volcanic arc<sup>19</sup>. This feature would provide a zone of hot, weak sub-arc lithosphere to concentrate crustal thinning, MCC formation, and ultimately continental breakup. Additionally, time may play a factor. The relatively short time since the onset of exhumation at Woodlark may be insufficient for crustal flow, which probably occurs at timescales of the order of 2–10 Myr depending upon viscosities and channel thickness<sup>4–6</sup>. This would explain why crust near the (older) MCCs has equilibrated, whereas crust in the young and active Woodlark rift has not. The Woodlark rift shows MCCs in development, before crustal flow has had a chance to complete.

The mantle velocities seen here suggest temperatures in excess of those predicted from pure-shear models of lithospheric thinning (Fig. 4b, orange line). (Hydration or enrichment from previous subduction may contribute to the low velocities here, although elevated temperatures and melt can explain most observations.) The P-wave anomalies locally exceed those found beneath mid-ocean ridges<sup>22</sup>, implying complete replacement of sub-continental mantle lithosphere by asthenosphere. Perhaps the pure-shear calculations underestimate mantle uplift because the pre-extensional crustal thickness beneath the MCCs may have been greater than in surrounding regions<sup>10</sup>, consistent with high pressures (5–6 kbar) at 4 Myr ago within the MCCs<sup>15</sup>. The additional mantle decompression may then suffice to produce buoyant melt as well as increased temperatures<sup>23</sup>, further contributing to buoyancy. Such mantle heating is also a component of previous magmatism-driven models for MCC formation here<sup>24</sup>, although such models elevate MCCs through crustal thickening, the opposite of what we observe.

As the mantle decompresses and approaches the peridotite solidus it should weaken, making this region susceptible to flow and further convective erosion of the mantle lithosphere beneath the MCCs<sup>25</sup>. Thus, mantle lithosphere appears to have been largely removed beneath much of the D'Entrecasteaux islands over a short timescale, providing a 'snapshot' of processes likely to lead to the opening of an ocean basin. □

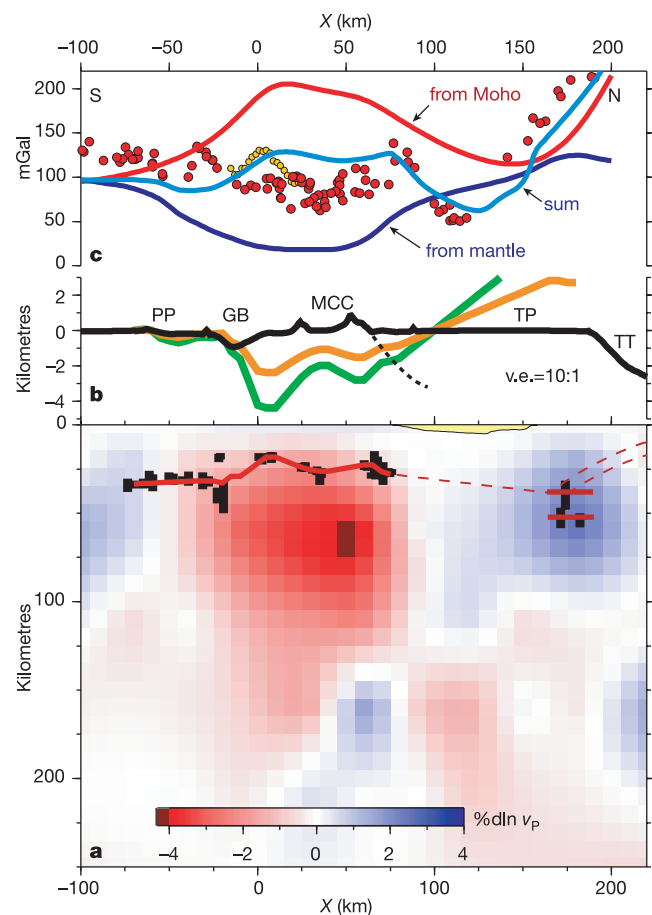


**Figure 4** North–south cross-section through the D'Entrecasteaux MCCs at 150.8° E; horizontal distance  $X = 0$  km corresponds to 10° S. **a**, Results of inversions. Colours represent perturbation to P velocities. Red line, Moho determined from receiver functions from stations west of 151.3° E smoothed at 10 km wavelength (and dashed where poorly constrained); vertical black bars, 95% confidence limits in individual measurements. For  $X > 170$  km, inferred Moho depth is based on fit to gravity of a thin elastic plate representing Trobriand trough underthrusting. Yellow patch, Trobriand basin incorporated in final gravity model. **b**, Topography, observed (black line) and predicted (green, orange). Abbreviations same as Fig. 1. Green line, topography predicted from Moho relief alone, assuming constant crustal and mantle density. Orange line, predicted initial subsidence<sup>30</sup> assuming mantle lithosphere thinning beneath each point exactly matching the crustal thinning. **c**, Bouguer gravity anomalies. Red and yellow circles, values observed on land and at sea, respectively. Red line, anomaly predicted from crustal thickness changes; dark purple line, anomaly predicted from mantle velocity anomalies; light blue line, sum of both, plus effect of Trobriand basin. Note general agreement in region where Moho depths and mantle velocities are well constrained by seismic experiment ( $-80$  km  $< X < 100$  km). v.e., vertical exaggeration.

Methods

Receiver functions

Teleseismic P wavetrains impinging upon the crust below stations give rise to a sequence of P-to-S conversions (Ps) and reverberations, which are isolated via receiver function techniques to constrain structure<sup>17</sup>. We generate receiver functions using standard frequency-domain methods. We select up to 91 low-noise events per station at a wide range of azimuths, and stack the filtered receiver functions into azimuthal bins 30° wide (see Supplementary Information). At all stations we observe a prominent positive pulse at 3–6 s lag following the direct P at zero lag (Fig. 2), interpreted to be the Ps conversion off the Moho. Azimuthal stacks of these waveforms are inverted for one or two parameters, typically the Moho depth and mid-crustal interface depth, using a waveform fitting approach<sup>26</sup> to produce crustal thickness estimates with 95% confidence limits from  $F$  tests. These inversions give estimates of crustal thickness at several Ps conversion points at the Moho around each station. Conversion times are transformed into depths using a one-dimensional velocity structure determined by a joint inversion of arrival times and hypocentres from 30 well-recorded local earthquakes. The inversion gives crustal P velocities of  $6.1 \text{ km s}^{-1}$  at depths  $> 10$  km, and upper-mantle  $P_n$  velocities of  $7.8 \text{ km s}^{-1}$ .

Travel time inversion

Residuals of teleseismic P waves are determined by waveform cross-correlation of the first cycle of incident P waveforms at frequencies of 0.15–1 Hz. From 102 events, 971 arrivals showed sufficient signal levels to use in inversion. Using standard methods<sup>27</sup> the differential residuals are inverted for velocity. Before inversion, the residuals are corrected

for variations in crustal thickness from receiver functions; velocities do not change in overall trend when corrections are not applied. The inversion is parameterized by a three-dimensional mesh spaced 30 km by 30 km horizontally and 50 km vertically, extending to 230 km depth. Experiments showed that variance reduction requires lateral heterogeneity only to 200 km depth, and that lateral resolution beneath the centre of the array is 30–40 km. In other words, the data set exhibits sensitivity to structures larger than 30–40 km within the upper 200 km of the Earth. Velocity anomalies in cross-section (Fig. 4) represent averages over three adjacent cells near 150.8° E longitude.

**Gravity calculations**

Gravity from variations in crustal thickness is calculated from the two-dimensional Moho geometry of Fig. 4a, assuming 400 kg m<sup>-3</sup> Moho density contrast. North of the northernmost station (*X* = 170 km), the Moho was forced to smoothly shallow to give 7-km-thick (oceanic) crust beneath the Trobriand trough (*X* = 244 km) in a mathematical form consistent with elastic flexure. The gravitational effect of a low-density contrast (−300 kg m<sup>-3</sup>) Trobriand basin was included (*X* = 70–180 km), based on its known geometry<sup>28</sup>. The anomaly due to mantle density variations ( $\delta\rho$ ) was derived from the estimated three-dimensional velocity perturbations ( $\delta v_p$ ), discretized into prisms of constant density. The conversion assumes  $\delta \ln \rho / \delta \ln v_p = 0.54$ , appropriate for dry pyrolyte at 2 GPa, based on a petrologically consistent database of mineral properties and equation-of-state calculations<sup>29</sup>. This conversion does not include effects of physical dispersion from attenuation<sup>18</sup>.

Received 10 January; accepted 17 July 2002; doi:10.1038/nature00990.

1. Lister, G. S. & Davis, G. A. The origin of metamorphic core complexes and detachment faults formed during Tertiary continental extension in the northern Colorado River region, U.S.A. *J. Struct. Geol.* **11**, 65–94 (1989).
2. Klemperer, S. L., Hauge, T. A., Hauser, E. C., Oliver, J. E. & Potter, C. J. The Moho in the northern Basin and Range Province, Nevada, along the COCORP 40 degrees N seismic-reflection transect. *Geol. Soc. Am. Bull.* **97**, 603–618 (1986).
3. McCarthy, J., Larkin, S. P., Fuis, G. S., Simpson, R. W. & Howard, K. A. Anatomy of a metamorphic core complex; seismic refraction/wide-angle reflection profiling in southeastern California and western Arizona. *J. Geophys. Res.* **96**, 12259–12291 (1991).
4. Block, L. & Royden, L. H. Core complex geometries and regional scale flow in the lower crust. *Tectonics* **9**, 557–567 (1990).
5. Kruse, S., McNutt, M., Phipps-Morgan, J., Royden, L. & Wernicke, B. Lithospheric extension near Lake Mead: A model for ductile flow in the lower crust. *J. Geophys. Res.* **96**, 4435–4456 (1991).
6. McKenzie, D., Nimmo, F., Jackson, J. A., Gans, P. B. & Miller, E. L. Characteristics and consequences of flow in the lower crust. *J. Geophys. Res.* **105**, 11029–11046 (2000).
7. Lister, G. S. & Baldwin, S. L. Plutonism and the origin of metamorphic core complexes. *Geology* **21**, 607–610 (1993).
8. Davies, H. L. & Warren, R. G. Origin of eclogite-bearing, domed, layered metamorphic complexes (“core complexes”) in the D’Entrecasteaux Islands, Papua New Guinea. *Tectonics* **7**, 1–21 (1988).
9. Abers, G. A. in *Non-Volcanic Rifting of Continental Margins: Comparison of Evidence from Land and Sea* (eds Wilson, R. C. L., Whitmarsh, R. B., Taylor, B. & Froitzheim, N.) 305–318 (Geological Society, London, 2001).
10. Taylor, B., Goodliffe, A. M. & Martinez, F. How continents break up: Insights from Papua New Guinea. *J. Geophys. Res.* **104**, 7497–7512 (1999).
11. Weisel, J. K., Taylor, B. & Karner, G. D. The opening of the Woodlark Basin, subduction of the Woodlark spreading system, and the evolution of northern Melanesia since mid-Pliocene time. *Tectonophysics* **87**, 253–277 (1982).
12. Ruppel, C. Extensional processes in continental lithosphere. *J. Geophys. Res.* **100**, 24187–24215 (1995).
13. Nyblade, A. A., Owens, T. J., Gurrrola, H., Ritsema, J. & Langston, C. A. Seismic evidence for a deep mantle thermal anomaly beneath east Africa. *Geology* **28**, 599–602 (2000).
14. Baldwin, S. L., Lister, G. S., Hill, E. J., Foster, D. A. & McDougall, I. Thermochronologic constraints on the tectonic evolution of active metamorphic core complexes, D’Entrecasteaux Islands, Papua New Guinea. *Tectonics* **12**, 611–628 (1993).
15. Hill, E. J. & Baldwin, S. L. Exhumation of high pressure metamorphic rocks during crustal extension in the D’Entrecasteaux Islands, Papua New Guinea. *J. Metamorph. Geol.* **11**, 261–277 (1993).
16. Ollier, C. D. & Pain, C. F. Active rising surficial gneiss domes in Papua New Guinea. *J. Geol. Soc. Aust.* **27**, 33–44 (1980).
17. Owens, T. J., Zandt, G. & Taylor, S. R. Seismic evidence for an ancient rift beneath the Cumberland Plateau, TN: a detailed analysis of broadband teleseismic P-waveforms. *J. Geophys. Res.* **89**, 7783–7795 (1984).
18. Karato, S. Importance of anelasticity in the interpretation of seismic tomography. *Geophys. Res. Lett.* **20**, 1623–1626 (1993).
19. Smith, I. E. in *Volcanism in Australasia* (ed. Johnson, R. W.) 275–286 (Elsevier, New York, 1976).
20. Martinez, F., Goodliffe, A. M. & Taylor, B. Metamorphic core complex formation by density inversion and lower-crust extrusion. *Nature* **411**, 930–934 (2001).
21. Achauer, U. et al. New ideas on the Kenya rift based on the inversion of the combined dataset of the 1985 and 1989/1990 seismic tomography experiments. *Tectonophysics* **238**, 305–329 (1994).
22. Toomey, D. R., Wilcock, W. S., Solomon, S. C., Hammond, W. C. & Orcutt, J. A. Mantle seismic structure beneath the MELT region of the East Pacific Rise from P and S wave tomography. *Science* **280**, 1224–1227 (1998).
23. McKenzie, D. & Bickle, M. J. The volume and composition of melt generated by extension of lithosphere. *J. Petrol.* **29**, 625–679 (1988).
24. Hill, E. J., Baldwin, S. L. & Lister, G. S. Magmatism as an essential driving force for formation of active metamorphic core complexes in eastern Papua New Guinea. *J. Geophys. Res.* **100**, 10441–10451 (1995).
25. Buck, W. R. & Su, W. Focused mantle upwelling below mid-ocean ridges due to feedback between viscosity and melting. *Geophys. Res. Lett.* **16**, 641–644 (1989).
26. Sheehan, A. F., Abers, G. A., Jones, C. H. & Lerner-Lam, A. L. Crustal thickness variations across the Colorado Rocky Mountains from teleseismic receiver functions. *J. Geophys. Res.* **100**, 20391–20404 (1995).

27. Roecker, S. W. in *Seismic Tomography Theory and Practice* (eds Iyer, H. M. & Hirahara, K.) 534–611 (Chapman and Hall, London, 1993).
28. Pinchin, J. & Bembrick, C. Cape Vogel Basin, PNG—tectonics and petroleum potential. *Bur. Min. Resour. Aust. Rec.* **32**, 31–37 (1985).
29. Hacker, B. R., Abers, G. A. & Peacock, S. M. Subduction factory I: Theoretical mineralogy, density, seismic wavespeeds, and H<sub>2</sub>O content. *J. Geophys. Res.* (in the press).
30. McKenzie, D. P. Some remarks on the development of sedimentary basins. *Earth Planet. Sci. Lett.* **40**, 25–32 (1978).

Supplementary Information accompanies the paper on Nature’s website (<http://www.nature.com/nature>).

**Acknowledgements**

The field effort in PNG would not have been successful without the efforts of S. Sioni, University of Papua New Guinea, J. Dickson, H. Sailasa and others of the Milne Bay Provincial Administration, PNG, and sub-district administrators throughout the province. Instruments and technical assistance were made available through the IRIS PASSCAL Instrument Center. The Geological Survey of Papua New Guinea gave permission to publish the gravity data on Fig. 4. We thank C. Ruppel for comments. This work was supported by the Geosciences Directorate of the National Science Foundation.

**Competing interests statement**

The authors declare that they have no competing financial interests.

Correspondence and requests for materials should be addressed to G.A. (e-mail: [abers@bu.edu](mailto:abers@bu.edu)).

.....  
**A mitochondrial remnant in the microsporidian *Trachipleistophora hominis***

**Bryony A. P. Williams\*, Robert P. Hirt\* & John M. Lucocq†  
 T. Martin Embley\***

\* Department of Zoology, The Natural History Museum, Cromwell Road, London SW7 5BD, UK

† School of Life Sciences, WTB/MSI complex, University of Dundee, Dundee DD1 5EH, UK

.....  
**Microsporidia are obligate intracellular parasites of several eukaryotes. They have a highly complex and unique infection apparatus but otherwise seem structurally simple<sup>1</sup>. Microsporidia are thought to lack typical eukaryotic organelles, such as mitochondria and peroxisomes. This has been interpreted as support for the hypothesis that these peculiar eukaryotes diverged before the mitochondrial endosymbiosis, which would make them one of the earliest offshoots in eukaryotic evolution<sup>2,3</sup>. But microsporidial nuclear genes that encode orthologues of typical mitochondrial heatshock Hsp70 proteins have been detected, which provides evidence for secondary loss of the organelle or endosymbiont<sup>4–6</sup>. In addition, gene trees and more sophisticated phylogenetic analyses have recovered microsporidia as the relatives of fungi, rather than as basal eukaryotes<sup>7–9</sup>. Here we show that a highly specific antibody raised against a *Trachipleistophora hominis* Hsp70 protein detects the presence, under light and electron microscopy, of numerous tiny (~50 × 90 nm) organelles with double membranes in this human microsporidial parasite. The finding of relictual mitochondria in microsporidia provides further evidence of the reluctance of eukaryotes to lose the mitochondrial organelle, even when its canonical function of aerobic respiration has been apparently lost.**

Molecular markers attest to a genetic heritage of the α-proteobacterial mitochondrial endosymbiont in microsporidia<sup>4–6,10,11</sup>; however, no experimental link has been shown between any of